J Electr Eng Technol.2015;10(1): 344-354
http://dx.doi.org/10.5370/JEET.2015.10.1.344

ISSN(Print) 1975-0102
ISSN(Online) 2093-7423

Features Extraction and Mechanism Analysis of Partial Discharge Development under Protrusion Defect

Yu-lin Dong*, Ju Tang†, Fu-ping Zeng and Min Liu***

Abstract – In order to study the development of partial discharge (PD) under typical protrusion defects in gas-insulated switchgear, we applied step voltages on the defect and obtained the φ–u and φ–n spectrograms of ultra-high frequency (UHF) PD signals in various PD stages. Furthermore, we extracted seven kinds of features to characterize the degree of deterioration of insulation and analyzed their values, variation trends, and change rates. These characteristics were inconsistent with the development of PD. Hence, the differences of these features could describe the severity of PD. In addition, these characteristics could provide integrated characteristics regarding PD development and improve the reliability of PD severity assessment because these characteristics were extracted from different angles. To explain the variation laws of these seven kinds of parameters, we analyzed the relevant physical mechanism by considering the microphysical process of PD formation and development as well as the distortion effect generated by the space charges on the initial field. The relevant physical mechanism effectively allocated PD severity among these features for assessment, and the effectiveness and reliability of using these features to assess PD severity were proved by testing a large number of PD samples.

Keywords: Protrusion defect, Partial discharge developing process, Feature extraction, Variation law, Mechanism analysis, Assessment

1. Introduction

Gas-insulated switchgear (GIS) is highly secure and reliable. During the process of its manufacture and long-term operation, however, inevitable defects in insulation result in partial discharge (PD) or insulation breakdown. This breakdown significantly affects social stability and economic development adversely [1]. PD is a main factor that causes insulation deterioration [2]. As such, PD severity can be monitored to determine the insulation condition of GIS and prevent insulation faults in reasonable and effective condition-based maintenance.

To develop a targeted maintenance strategy for GIS, we must identify defect types and evaluate PD severity. However, the existing research of PD online monitoring focus on signal de-noising [3-6], PD sources location [7] and pattern recognition [8-11], PD severity assessment was rarely involved. To evaluate PD severity, the insulation dielectric property of GIS is the basic characteristic of the PD development process. SF_6 gas acts as the insulation dielectric of GIS and differs from solid dielectric. Moreover, it does not age. Therefore, the developing process of PD in GIS varies from that in solid dielectric significantly. To understand the insulation condition of GIS, studying the development of PD in GIS is urgent and necessary.

As a result of different degrees of insulation deterioration, the local electric field is distorted to different degrees. Thus, the characteristics of PD signals vary significantly in the development of PD. The investigation of PD development process mainly aims to extract the PD characteristics that guide equipment condition-based maintenance. Research has determined the statistical characteristics of PD, including discharge times, amplitudes, and phases [12-18]. According to the analysis, the ratios of discharge times between positive and negative half-cycles are regular, as well as the ratios of discharge times and amplitudes. These features are closely related to PD severity. However, they cannot represent the sole criterion in the diagnosis and assessment of PD severity [16], although discharge times and amplitudes display a certain monotonic property and regularity, which are closely related to the development of PD. Thus, we should also consider other reference characteristics. In brief, we cannot characterize PD severity precisely through only a single or a few features without properly understanding the developing process of PD.

Therefore, we examined PD development in GIS under typical protrusion defects systematically. To characterize PD severity, we extracted seven kinds of features according to the differences in ultra-high frequency (UHF) PD

† Corresponding Author: State Key Laboratory of Power Transmission Equipment & System Security and New Technology Chongqing University, Chongqing, China; School of Electrical Engineering, Wuhan University, China. (cqtangju@cqu.edu.cn)
* State Key Laboratory of Power Transmission Equipment & System Security and New Technology Chongqing University, Chongqing, China. (dongyulin@foxmail.com)
** School of Electrical Engineering, Wuhan University, China. (fuping.zeng@gmail.com)
Received: July 22, 2014; Accepted: September 16, 2014

characteristics in different PD stages, namely, the maximum pulse amplitudes of PD, discharge times, maximum ratios of adjacent PD pulse amplitudes, average time intervals of adjacent PD pulses, maximum time intervals of adjacent PD pulses, equivalent cumulative discharge quantities, and signal entropies. Besides, we analyzed the microphysical process of the formation and development of PD together with the distortion effect caused by space charges to determine the variation laws of the seven parameters. Finally, the effectiveness and reliability of using these features to assess PD severity were proved by testing a large number of PD samples.

2. Experimental Study

2.1 Schematic of the experiment

As shown in Fig. 1, T1 is the voltage regulator, T2 is the test transformer (YDTCW-1000/2×500) without corona, C1/C2 is the capacitive divider (TAWF-1000/600), and R is the protective resistor (GR1000-1/6). PD signals were acquired by a microstrip antenna (bandwidth: 340 MHz to 440MHz; center frequency: 390MHz) [19] and were displayed and stored on a digital oscilloscope (analog bandwidth: 1GHz; maximum sampling rate: 20GS/s; memory depth: 48MB). Based on the characteristics of typical metal protrusion defect, we designed a needle-plate model (distance: 5mm, radius of curvature: 0.3mm) to simulate the protrusion defect [20]. The model was placed in a simulated GIS, which was filled with 0.4MPa of SF_6 gas.

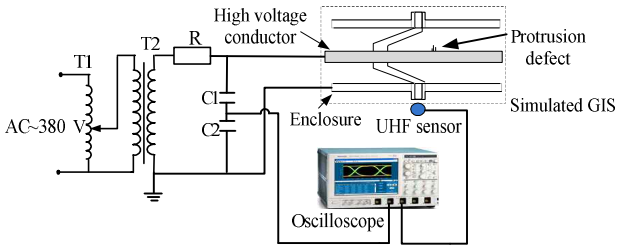

Fig. 1. Schematic of the experimental circuit

2.2 Experimental method

To investigate the developing process of PD under protrusion defect, we can apply the test voltage in two ways, namely, the constant and step voltage methods [17]. However, the constant voltage method is time-consuming; hence, it is unsuitable for regular experimental studies. In contrast, the step voltage method accelerates defect deterioration through high-voltage stress. It can not only simulate PD development, but also obtain much effective data within a short time period. Consequently, we used the step voltage method to study the development of PD in GIS under protrusion defect.

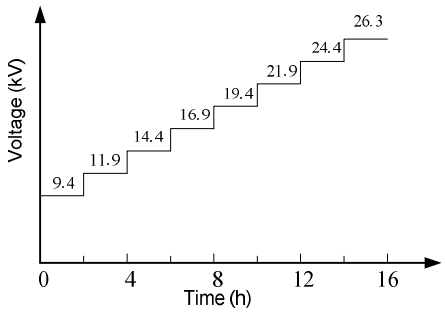

Fig. 2. Experimental voltages and durations

The results of previous tests showed that although the applied voltage was high enough to induce defect breakdown, the simulated GIS did not generate PD because of its high insulating strength. All experimental PD signals were induced by the needle-plate defect. In the experiment, the applied voltage was increased slowly until stable PD signals were detected. The initial discharge voltage was measured at 9.4kV. The single PD pulse waveform was acquired when the oscilloscope sampling rate was set at 5GS/s. And the oscilloscope sampling rate was set at 50MS/s to acquire the PD signals in each power cycle per second. Each PD sample underwent 100 power cycles, and 50 samples were obtained. The applied voltages were increased by 2.5kV every 2h, and all of the PD signals of each voltage were collected. At 26.3kV, we heard a strong corona. At 27.6kV, the defect broke down. To ensure oscilloscope security, the PD signals under 26.3kV were derived as the representative PD signals near the defect breakdown instead of the PD signals under 27.3kV. Fig. 2 depicts the experimental voltages and durations.

3. Analysis of Discharge Spectrograms

To study the PD development process in a simulated GIS under needle-plate defect, we conducted a total of five experiments. The results of these experiments were repeatable and the variation tendency of the PD evolution was similar. As such, we analyzed the PD development process using only one set of test results. Fig. 3 displays a typical UHF PD pulse waveform and its frequency spectrum. Fig. 4 displays the φ–u and φ–n spectrograms of the UHF PD signals.

PD pulses first appeared near the peak voltages in negative half-cycles, which mainly distributed from 250° to 310°. In contrast, few PD pulses were observed in positive half-cycles, which mainly distributed from 75° to 105°. PD pulses amplitudes in negative half-cycles were evidently bigger than those in positive half-cycles, as shown in Fig. 4(a). When the voltage reached 11.9kV, PD pulses amplitudes increased significantly, and the maximum PD pulse amplitude was twice that of the initial discharge voltage. In addition, discharge times in negative half-cycles increased significantly. PD pulses

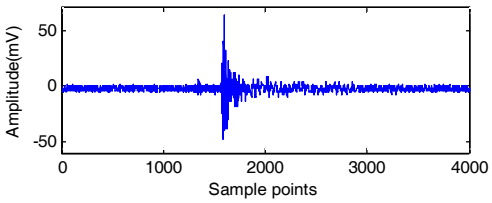

(a) Time-domain waveform

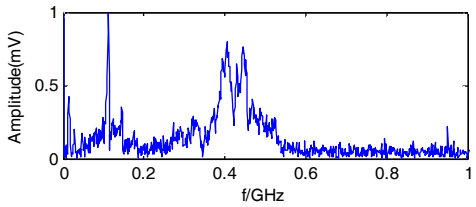

(b) Frequency spectrum

Fig. 3. A single UHF PD signal

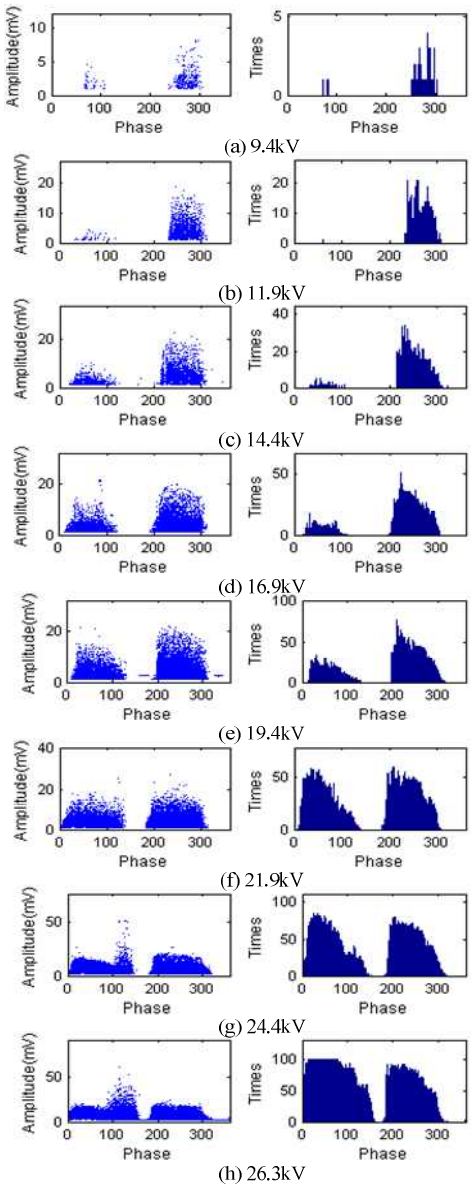

(a) 9.4kV
(b) 11.9kV
(c) 14.4kV
(d) 16.9kV
(e) 19.4kV
(f) 21.9kV
(g) 24.4kV
(h) 26.3kV

Fig. 4. *φ–u* and *φ–n* spectrograms at different PD stages

were concentrated around 270°, and discharge phases ranged from 230° to 320°. However, the determining PD pulses in positive half-cycles remained challenging, as presented in Fig. 4(*b*).

When the voltage reached 14.4kV, the amplitudes and times of PD pulses increased sharply in both positive and negative half-cycles. Furthermore, PD pulses amplitudes in positive half-cycles reached approximately 10mV. However, discharge times remained short in these half-cycles and far shorter than those in negative half-cycles. Moreover, *φ–n* spectrogram of negative half-cycles was approximately triangular and deviated to 180°. In contrast, the *φ–n* spectrogram of positive half-cycles had no clear inclination.

Although discharge times in positive and negative half-cycles increased significantly at a voltage of 16.9kV, those in positive half-cycles were far shorter than those in negative half-cycles. In negative half-cycles, PD pulses amplitudes did not increase significantly; however, they did so in positive half-cycles. Furthermore, the amplitudes of some PD pulses in positive half-cycles exceeded those in negative half-cycles. In addition, the *φ–n* spectrogram of negative half-cycles continually deviated to 180°, and several PD pulses were observed near 200°.

In both positive and negative half-cycles, PD pulses amplitudes and discharge times increased at a voltage of 19.4kV. The *φ–n* spectrogram of negative half-cycles continually deviated to 180°. Furthermore, the triangular *φ–n* spectrogram of positive half-cycles was skewed toward 0°. As the voltage increased to 21.9kV, the *φ–u* spectrograms of positive and negative half-cycles were trapezoidal. The value of the maximum PD pulse amplitude of positive half-cycles was approximately equal to that of negative half-cycles, so as the distribution width of discharge phase. Discharge phase of positive half-cycles ranged from 5° to 125°, whereas the phase of negative half-cycles ranged from 190° to 310°. In this discharge stage, the discharge times increased sharply, and the maximum discharge times in positive half-cycles were basically equal to those in negative half-cycles. The *φ–n* spectrogram of positive half-cycles is continually skewed toward 0°.

When the voltage increased to 24.4kV, PD pulses appeared at 0°. The amplitudes of PD pulses ranging from 0° to 100° did not increase significantly, whereas those of PD pulses ranging from 100° to 125° did so in areas with only a few pulses. The maximum PD pulse amplitude reached 53mV. Moreover, PD pulses of positive half-cycles mainly distributed in areas near 0°, and the maximum discharge times were observed around 30°. The peak of the *φ–n* spectrogram of positive half-cycles was clear. The discharge times were maintained at approximately 25 times in the area ranging from 100° to 125°. In contrast, PD pulse amplitudes in negative half-cycles did not increase sharply as the discharge times increased continually. Thus, the distribution of discharge pulses in the *φ–u* spectrogram became uniform at each discharge phase.

When the voltage reached 26.3kV, the sound of corona could be heard. Discharge intensified and approached the breakdown stage. In this stage, PD pulses were almost observed in all phases, although discharge times in the phases ranging from 155° to 175° and 320° to 360° were far shorter than in the rest phases, as exhibited in Fig. 4(*h*). Furthermore, the width of the main discharge phase in positive half-cycles was significantly greater than that in negative half-cycles. In positive half-cycles, the main phase ranged from 0° to 155° in positive half-cycles and from 180° to 300° in negative half-cycles. In addition, discharge times in positive half-cycles were distinctly larger than those in negative half-cycles. Discharge times reached 100 times in the phase ranging from 5° to 80°, which suggests that PD pulses appeared at that phase in every power cycle. In the phase ranging from 100° to 125°, PD pulses amplitudes continued to increase. The phase expanded to both sides, which had ranged from 80° to 140°. However, the discharge phase and the amplitudes of discharge pulses in other phase ranging from 0° to 80° and 180° to 300° had no significant increase.

4. Discharge features and their variation laws

4.1 Features extraction

4.1.1 Maximum ratio of adjacent PD pulse amplitudes R_{max}

PD pulses amplitudes increased with the development of PD. By analyzing the PD pulses amplitudes of positive and negative half-cycles, we observed that the ratio of adjacent PD pulses amplitudes possessed meaningful properties that could direct the assessment of PD severity. Fig. 5 shows a schematic of the PD pulses in a power cycle. In positive and negative half-cycles, R_{max} values were calculated using Eqs. (1) and (2), respectively.

$$R_{max}^{+}=max\left\{\begin{array}{l}\dfrac{u_1^+}{u_2^+},\ max\left(\dfrac{u_2^+}{u_1^+},\dfrac{u_2^+}{u_3^+}\right),\ max\left(\dfrac{u_3^+}{u_2^+},\dfrac{u_3^+}{u_4^+}\right),\\ \ldots,max\left(\dfrac{u_{N^+-1}}{u_{N^+-2}},\dfrac{u_{N^+-1}}{u_{N^+}}\right),\dfrac{u_{N^+}}{u_{N^+-1}}\end{array}\right\} \quad (1)$$

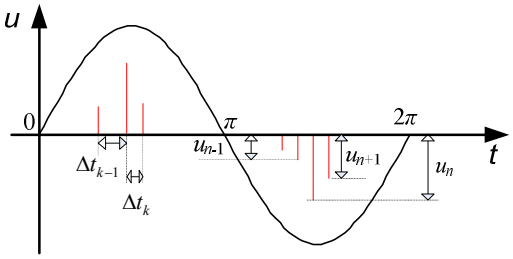

Fig. 5. Schematic of PD pulses in a power cycle

$$R_{max}^{-}=max\left\{\begin{array}{l}\dfrac{u_1^-}{u_2^-},max\left(\dfrac{u_2^-}{u_1^-},\dfrac{u_2^-}{u_3^-}\right),max\left(\dfrac{u_3^-}{u_2^-},\dfrac{u_3^-}{u_4^-}\right),\\ \ldots,max\left(\dfrac{u_{N^--1}}{u_{N^--2}},\dfrac{u_{N^--1}}{u_{N^-}}\right),\dfrac{u_{N^-}}{u_{N^--1}}\end{array}\right\} \quad (2)$$

Where N^+ and N^- represent the discharge times of positive and negative half-cycles in a power cycle, respectively; u_i^+ (i=1,2,…,N^+) and u_i^- (i=1,2,…,N^-) denote the PD pulses amplitudes of positive and negative half-cycles in a power cycle, respectively; and R_{max}^+ and R_{max}^- indicate the maximum ratios of the adjacent PD pulses amplitudes of positive and negative half-cycles in a power cycle, respectively.

4.1.2 Time interval of adjacent PD pulses ΔT

Based on the φ–u and φ–n spectrograms, the intensities of PD pulses and ΔT varied in positive and negative half-cycles with PD development. Moreover, discharge phases of both positive and negative half-cycles expanded in PD developing process. ΔT of negative half-cycles was similar to that of positive half-cycles, and both changed regularly. To describe the fingerprint information at different PD stages, we extracted three features by calculating Eq. (3) to (5).

$$\overline{\Delta T}^{+}=\frac{1}{N^+-1}\sum_{i=1}^{N^+-1}\Delta t_i^+ \quad (3)$$

$$\overline{\Delta T}^{-}=\frac{1}{N^--1}\sum_{i=1}^{N^--1}\Delta t_i^- \quad (4)$$

$$\Delta T_{max}=max\left(\Delta t_1,\Delta t_2,\ldots,\Delta t_{N-1}\right) \quad (5)$$

Where N^+ and N^- are the discharge times of positive and negative half-cycles in a power cycle, respectively; Δt_i^+ (i=1,2,…, N^+) and Δt_i^- (i=1,2,…, N^-) are the intervals of the adjacent PD pulses of positive and negative half-cycles in a power cycle, respectively; $\overline{\Delta T}^{+}$ and $\overline{\Delta T}^{-}$ are the average intervals of the adjacent PD pulses of positive and negative half-cycles in a power cycle, respectively; N denotes the discharge times of one power cycle; Δt_i (i=1,2,… N–1) represents the intervals of adjacent PD pulses in a power cycle; and ΔT_{max} is the maximum interval of PD pulses in a power cycle.

4.1.3 Equivalent cumulative discharge quantities Q_{acc}

With the increase in PD intensity, the quantities of discharge per unit time increase. As a result, PD damage to the insulation is serious. Hence, discharge quantities within a certain period can characterize PD severity. Research has indicated that the apparent discharge quantities had quadratic integral relation with the pulses amplitudes of UHF PD signals [21, 22]. Q_{acc} is calculated using Eq. (6).

$$Q_{acc} = \sum_{i=1}^{N} u_i^2 \quad (6)$$

Where N represents the discharge times within a power cycle and u_i is the i-th PD pulse amplitude.

4.1.4 Signal entropy En

For a PD pulse sequence within a power cycle, signal complexities can represent the differences in PD pulses amplitudes, discharge times, and discharge phases in various PD stages. Information complexity is denoted by information entropy, where an increase in the former enlarges the latter [23]. *En* can be computed using Eq. (7).

$$En = -\sum_{i=1}^{N}\left(\left(u_i \sum_{i=1}^{N} u_i\right)\log\left(u_i \sum_{i=1}^{N} u_i\right)\right) \quad (7)$$

Where N indicates the discharge times within a power cycle and u_i is the i-th PD pulse amplitude.

4.2 Variation laws of the features

4.2.1 Maximum PD pulse amplitude u_{max}

Fig. 6 depicts the variation curves of u_{max} in negative and positive half-cycles. Each data point in the curves is the average value of 100 power cycles. In negative half-cycles, u_{max} was increasingly saturated. Specifically, u_{max} increased slightly from 11.9kV to 16.9kV. It then reached a saturation value. In positive half-cycles, u_{max} increased exponentially throughout the entire PD developing process. In the range of the initial discharge voltage to 19.4kV, u_{max} in positive half-cycles was less than that in negative half-cycles. However, u_{max} in positive half-cycles exceeded that in negative half-cycles and increased rapidly when the voltage was above 19.4kV. When the voltage reached 26.3kV, u_{max} approached 65mV.

4.2.2 Discharge times N

Fig. 7 displays the variation curves of the average N values of positive and negative half-cycles of a power cycle at different PD stages. In both positive and negative half-cycles, N increased, although the discharge times of negative half-cycles increased relatively gradually. In the initial discharge stage, N of positive half-cycles was small and increased slowly. However, when the applied voltage reached 16.9kV or above, N of positive half-cycles almost doubled. In addition, it increased significantly and exceeded that of negative half-cycles when the applied voltage reached the breakdown voltage.

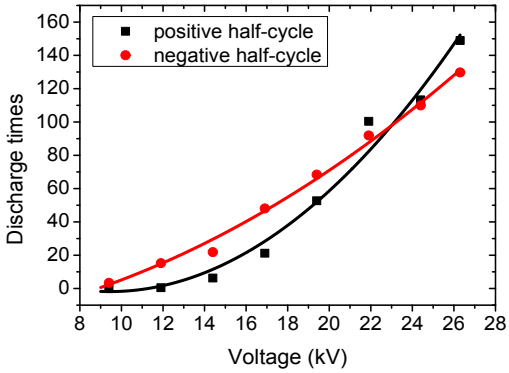

Fig. 7. Discharge times of PD pulses

4.2.3 Maximum ratio of adjacent PD pulses amplitudes R_{max}

Fig. 8 exhibits the variation curves of R_{max} in negative and positive half-cycles. Each data point in the curves is the average value of 100 power cycles. In both positive and negative half-cycles, the variation laws of R_{max} were similar to those of u_{max}. R_{max} of positive half-cycles increased significantly, especially at a voltage exceeding 21.9kV. However, R_{max} of negative half-cycles was increasingly saturated, and the increment in total ratios was small. In positive half-cycles, however, R_{max} growth was steeper than that of u_{max} when the applied voltage reached to the breakdown voltage. In negative half-cycles, the growth of R_{max} was gentler than that of u_{max} in negative half-cycles during the PD development process.

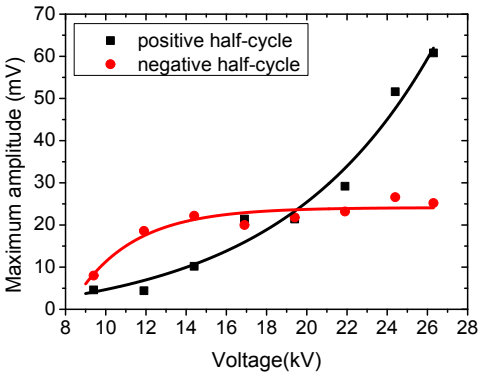

Fig. 6. Maximum PD pulse amplitudes

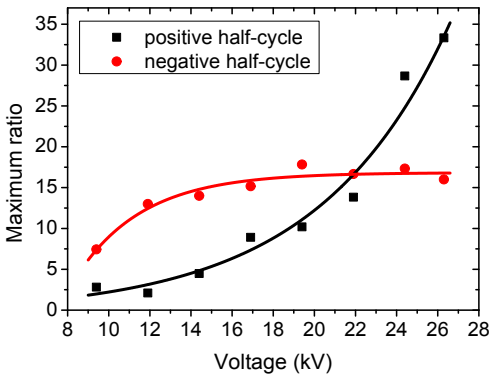

Fig. 8. Maximum ratio of adjacent PD pulses amplitudes

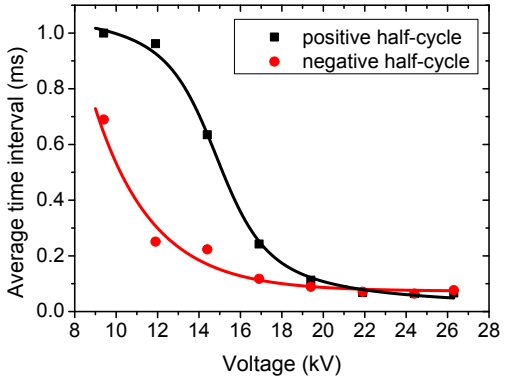

Fig. 9. Average time intervals of adjacent PD pulses

4.2.4 Average time intervals of adjacent PD pulses $\overline{\Delta T}$

Fig. 9 shows the variation curves of the $\overline{\Delta T}$ values of the positive and negative half-cycles in 100 power cycles. In negative half-cycles, $\overline{\Delta T}$ decayed exponentially and $\overline{\Delta T}$ decayed in S-shaped curve in positive half-cycles. Furthermore, $\overline{\Delta T}$ was greater in positive half-cycles than that in negative half-cycles. With the development of PD and the nearness of the insulation defect to the breakdown stage, these differences gradually narrowed until they were basically equal.

4.2.5 Maximum time intervals of adjacent PD pulses ΔT_{max}

According to φ–n spectrograms, ΔT_{max} of a power cycle is identical to the time interval of two recent PD pulses originating from positive and negative half-cycles, respectively. ΔT_{max} represents the change trend of the phase distribution of positive and negative half-cycles to some extent. Fig. 10 displays the variation curve of ΔT_{max}, and each data point is the average value of 100 power cycles. With the development of PD, ΔT_{max} decreased, which indicated that the phase of positive half-cycle gradually approached that of negative half-cycle.

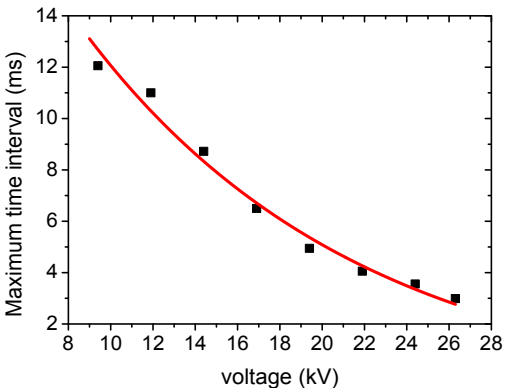

Fig. 10. Maximum time interval of adjacent PD pulses in a power cycle

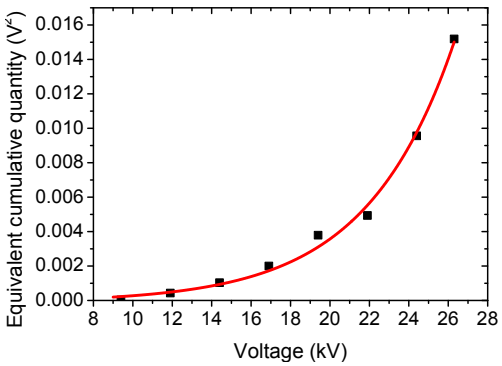

Fig. 11. Equivalent cumulative quantities in different PD stages

4.2.6 Equivalent cumulative quantities Q_{acc}

Fig. 11 presents the variation curve of the averaged Q_{acc} values of a power cycle. Q_{acc} increased exponentially with the development of PD intensity. The increase in PD intensity was induced by the increase of the applied voltage. Furthermore, Q_{acc} increases rapidly when the insulation degraded severely, especially near the breakdown stage.

4.2.7. Signal entropy En

At different PD stages, the average *En* of a power cycle increased exponentially, as shown in Fig. 12. As the applied voltage increased, PD intensified. Moreover, PD signals were complicated, thus enriching information. Hence, *En* increased during the developing process of PD.

In conclusion, the variation laws of these features vary with the development of PD. Furthermore, these features provide rich, integrated information for PD severity assessment. As such, the differences in these features can be used to deconstruct and assess the severity of PD. Given the fuzzy division of PD severity, the application of a single feature to describe different PD stages is unreliable. But, the unreliability can be removed by using these features to assess the severity of PD.

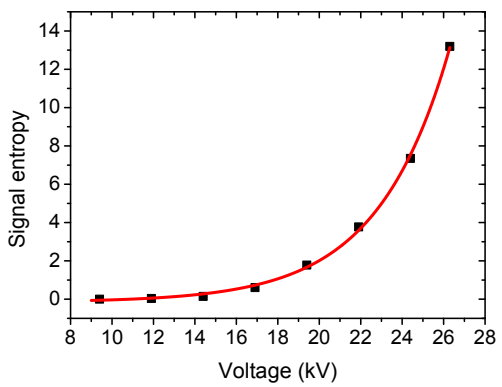

Fig. 12. Entropy feature in different PD stages

5. Mechanism Analysis of the Variation Laws of the Features

During the developing process of PD, numerous charged particles are formed in the needle-plate gap as a result of electron emission, SF_6 ionization, and attachment. Positive and negative particles move in opposite directions under the action of electric field. They either strengthen or weaken the front electric field of the needle electrode. Fig. 13 illustrates electric field distribution under the influence of space charges in positive and negative half-cycles, respectively. E_{in} is the initial electric field and E_{com} is the composite electric field under the influence of space charges [24-26].

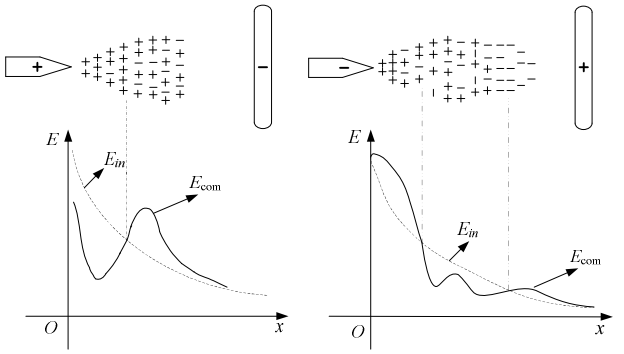

(a) Positive half-cycle (b) Negative half-cycle

Fig. 13. Electric field distribution under the influence of space charges

5.1 Change mechanism of u_{max}

The local electric field near the tip is too weak to ionize SF_6 gas molecules due to its high dielectric strength. Therefore, the applied voltage must be adequately high. The injection of charged particles into the electrode or electrons emission from the electrode generates a certain pulse current and excites the UHF electromagnetic wave. As such, the signal amplitude of UHF PD increases with the increase of the pulse current amplitude.

In negative half-cycles, PD is easily produced because positive space charges enhance the electric field near the tip. When the voltage range from the initial discharge voltage to 16.9kV, the increase of the applied voltage strengthens the local electric field near the tip and improves the ionization of SF_6. This intensified ionization results in the enhanced absorption of positive ions into the needle electrode and electrons emission of the needle electrode per unit time. Thus, u_{max} increases with the increase of the applied voltage. Furthermore, adequate high voltage causes secondary electrons to neutralize some of the positive ions near the needle electrode, although the positive ions are likely to be absorbed into the cathode. These secondary electrons are formed from the cathode surface stricken by positive ions. The number of positive ions absorbed into the cathode and the number of electrons emitted from the cathode per unit time reach a saturation value when the concentration of positive ions is at or above a certain level because of their large mass and bulk, slow migration, and high probability of collision among these ions. Hence, u_{max} is increasingly saturated with the development of PD in negative half-cycles.

In positive half-cycles, the residual positive space charges near the tip impair the local electric field. Therefore, the initial discharge voltage of positive half-cycles is higher than that of negative half-cycles. When the applied voltage is low, u_{max} of positive half-cycles is small due to the weak ionization of SF_6. As the voltage increases, SF_6 ionization intensifies and produces abundant charged particles. Because the mass of electron is much lighter than that of positive ion, electrons are rapidly absorbed into the anode during ionization. Thus, the increase of the applied voltage enhances u_{max}. In addition, the electric field established by the increased applied voltage accelerates the migration of all positive ions toward the cathode and diminishes the impairing effect of positive space charges. Positive space charges enhance the local electric field near the tip. Furthermore, this electric field increases u_{max}. Consequently, this rapid ionization sharply enhances $u_{\max}$ when the voltage is close to the threshold voltage of the breakdown.

5.2 Change mechanism of N

In negative half-cycles, positive ions migrate to the needle electrode and some of them disappear in the needle electrode, whereas electrons migrate toward the plate electrode. Some of these electrons neutralize some positive space charges, whereas other electrons attach to the neutral molecule. Thus, the strengthening effect of positive space charges on the initial electric field weakens. As a result, PD ceases. When the voltage is adequately high, the SF_6 gas molecules ionize to generate PD pulses again. As is known, a high voltage forms a strong electric field, thus simplifying PD. Meanwhile, the electric field built by the applied voltage and space charges quickly reaches a critical level. As such, the next PD pulse generate in a short time. Therefore, a high voltage intensifies PD pulses and increases N.

Similar to the negative half-cycles, a high voltage increases instantaneous voltage increments in an equal period in positive half-cycles, as well as N. Moreover, the electric field constructed by the increased voltage accelerates the migration of positive ions toward the cathode. This process weakens the effect of space charges. Hence, N increases with the increase of the applied voltage.

The differences of the increase in N values are caused by positive space charges. In positive half-cycles, positive space charges weaken the local electric field, which complicates PD. The applied voltage must increase to facilitate SF_6 ionization. Hence, N of positive half-cycles is

smaller than that of negative half-cycles. When the voltage approaches the breakdown voltage, the impairing effect caused by positive charges will decrease sharply with the decline of instantaneous value of sinusoidal voltage, because positive ions migrate toward the cathode. In contrast, this strengthening effect is always weak in negative half-cycles. As such, the compound field reduces more significant than that in positive half-cycles as the instantaneous voltage declines. This reduction complicates PD. Consequently, N of positive half-cycles exceeds that of negative half-cycles near the breakdown stage.

5.3 Change mechanism of R_{max}

In positive half-cycles, each strong PD generates numerous positive ions, which can weaken the electric field around the needle electrode. Under the influence of positive space charges, the compound electric field reduces and discharges are weak when the instantaneous voltage reaches to the critical voltage value. Therefore, each significant PD always produces many small PD pulses. The weakening effect of positive space charges decreases after a period because of the migration of positive ions. A significant PD pulse generates again when the instantaneous voltage increases. Therefore, the electric field is strengthened when the applied voltage is near the peak. Furthermore, ionization intensifies and the amplitudes of PD pulses increase. As a result of the weakening effect of mass positive space charges on the local electric field, the pulse amplitudes that follow the significant PD pulse are not significantly enhanced. Therefore, R_{max} increases exponentially.

In negative half-cycles, u_{max} is increasingly saturated with the increase of the applied voltage. After each intense discharge, numerous secondary electrons produce when positive ions strike the cathode surface and migrated to the anode. Some electrons neutralize some of positive space charges and other electrons attach to neutral molecules to form negative ions. Negative ions impair the strengthening effect of positive ions on the local electric field. Therefore, the PD pulse amplitude beside the significant amplitude of PD pulse remains small. R_{max} is also increasingly saturated.

5.4 Change mechanism of $\overline{\Delta T}$

When the applied voltage is low in positive half-cycles, PD generation is difficult because of the weakening effect of positive space charges on the local electric field near the tip. In order to ionize SF_6 gas molecules, the instantaneous voltage value must increases. As such, $\overline{\Delta T}$ is relatively large. In negative half-cycles, the positive space charges strengthen the local electric field, thus simplifies PD. Hence, $\overline{\Delta T}$ of these half-cycles is smaller than that of the positive half-cycles. As the applied voltage increases, the compound electric field near the tip is strengthened, thereby resulting in easy PD generation. Therefore, $\overline{\Delta T}$ gradually decreases in both positive and negative half-cycles, so as the differences between $\overline{\Delta T}$ of positive half-cycles and that of negative half-cycles.

5.5 Change mechanism of ΔT_{max}

ΔT_{max} values are equal to the interval of the closest PD pulses of positive and negative half-cycles. In positive half-cycles, some of positive ions remain near the tip after each discharge. In positive half-cycles, as discharge intensifies with the increase of the applied voltage, the number of residual positive ions increases. In negative half-cycles, the strengthening effect of positive space charges accumulated from positive half-cycles in the electric field near the tip increases. Simultaneously, PD generation is simplified and the PD pulses approach 180°. Therefore, ΔT_{max} values decrease.

5.6 Change mechanism of Q_{acc}

Q_{acc} is the quadratic sum of all PD pulse amplitudes in a power cycle. With the increase of the applied voltage, the local electric field near the tip is increasingly strengthened. In the process of discharge, ionization intensifies and the amount of charges transferred as discharge increase. This phenomenon indicates that PD pulse amplitudes and discharge times increase. Therefore, Q_{acc} increases with the development of PD.

5.7 Change mechanism of *En*

Entropy is a measurement of complexity. In PD development, a high applied voltage intensifies ionization near the tip. With the strong electric field, the velocity of charged particles increases. The movements of these particles are disorganized as a result of violent collisions. PD pulses are intensified with the increase of discharge times and PD pulse amplitudes. Moreover, the distribution of discharge phase expands. In brief, PD pulses in a power cycle are increasingly complex. Finally, *En* increases with the development of PD.

In conclusion, all of the change characteristics of these features are closely related to the electric field built by the applied voltage and space charges during the development of PD. In the process, positive space charges can be accumulated and distort the initial electric field. Furthermore, PD pulses are produced when positive ions or electrons are absorbed into the electrode, or electrons are emitted from the electrode. The essential characteristics of positive ions and electrons vary and result in the dissimilar variation laws of these features of negative and positive half-cycles. In view of the close relationship of the features with the development of PD and considering the differences among the features, we can utilize the seven kinds of features to deconstruct and assess PD severity.

6. Evaluation of the Effectiveness of the Features

In order to evaluate the effectiveness of the seven kinds of features extracted in this paper, the degree of PD severity is divided into three stages, namely normal state, attention state and warning state, as shown in Table 1. In the normal state, there is a small amount of stable PD pulses in negative half-cycles and no obvious discharge in positive half-cycle, or even no discharge in the whole frequency-cycles. In the attention state, the amplitudes of PD pulses of negative half-cycles increase and have a tendency toward a saturation value. Besides, a small amount of weak PD pulses appear in positive half-cycle, and their amplitudes and discharge times are much smaller than that in negative half-cycles. In the warning state, the amplitudes of PD pulses in negative half-cycles reach to a saturate value, and discharge times increased significantly. While, both the amplitudes and discharge times of PD pulses in positive half-cycles increase sharply, and begin to exceed that in negative half-cycles.

Table 1. Definition of the severity degrees of PD

Voltage/kV	State	State description	maintenance strategy
9.4/11.9	Normal	Initial discharge stage	Regular maintenance
14.4/16.9/ 19.4	Attention	Discharge development stage	Real-time detection or minor overhaul
21.9/24.4/ 26.3	Warning	Pre-breakdown stage	Overhaul or replacement of equipment

Support vector machine (SVM) is an intelligent algorithm based on the structural risk minimization machine learning theory [27]. It overcomes the problems, such as over-learning, inadequate learning and local convergence, and achieves an excellent balance between learning accuracy and generalization ability, which make it suitable for solving the small sample, high-dimensional and nonlinear model case in classification and prediction problems, and has been widely applied in the transient stability assessment of power system. Therefore, SVM classifier and the "one to one" classification method were adopted in this paper to assess the severity of PD. Gaussradial basis kernel function was chosen as kernel function of SVM, as displayed in Eq. (8):

$$K(x,y)=\exp(-\frac{\|x-y\|^2}{2\sigma^2}) \tag{8}$$

Where, σ is its default value $1/N_r$, and N_r is the dimension of features. The penalty factor C is 10.

Twenty samples are selected randomly as the training samples under each voltage, and the rest are treated as testing samples. In order to conduct comparative analysis, two kinds of the input feature $\boldsymbol{F}_1$ and $\boldsymbol{F}_2$ are set. $\boldsymbol{F}_1$ contains all the seven kinds of features extracted in this paper. $\boldsymbol{F}_2$ is normal statistical discharge characteristics, namely $\boldsymbol{F}_2$=[u_{max}^{+} u_{max}^{-} N^{+} N^{-}]. The final test results are shown in Table 2.

It can be obtained that the accuracy of PD severity evaluation increased significantly when adopt the features $\boldsymbol{F}_1$ instead of $\boldsymbol{F}_2$, and all the correct rates are above 91%, so it is effective to use the seven kinds of features extracted in this paper to assess PD severity and it would have a high assessment reliability compare to using a single feature or a few features to assess the PD severity.

Table 2. Assessment results of the severity of PD

State degrees	Training samples	Testing samples	Accuracy/%	
			$\boldsymbol{F}_1$	$\boldsymbol{F}_2$
Normal	20/20	30/30	100	100
Attention	20/20/20	30/30/30	97.78	80
Warning	20/20/20	30/30/30	91.11	86.67

7. Conclusion

1) The characteristics of the spectrograms vary at different PD stages. In the initial discharge stage, PD pulses are first observed in negative half-cycles. As the applied voltage increases, PD pulses appear in positive half-cycles. In these half-cycles, N and u_{max} are smaller than those in negative half-cycles. However, N and u_{max} increase significantly in positive half-cycles and exceed those in negative half-cycles when the applied voltage reaches to the breakdown voltage. During the development process of PD, u_{max} increases slowly in negative half-cycles, whereas N increases significantly. The distribution of discharge phase expands gradually, and φ–n spectrograms of positive and negative half-cycles deviate to 0° and 180°.

2) In positive half-cycles, u_{max} and R_{max} increase exponentially, whereas they are increasingly saturated in negative half-cycles. Moreover, N typically increases with the development of PD in both positive and negative half-cycles. ΔT decays exponentially in both positive and negative half-cycles. ΔT_{max} decreases significantly, although it does not display typical exponential decay. Q_{acc} and En increase exponentially with the development of PD.

3) The strong electric field established by the applied voltage and space charges induces SF_6 ionization and PD generation. On the basis of the microphysical process of PD formation and development, this paper elucidates the effect mechanism of space charges on each feature. By considering the PD pulses, we deduce that the intrinsic differences between electrons and positive ions result in variations in the features of positive and negative half-cycles. Subsequently, we explain the relationship between the features and the development of PD, which confirms that the seven kinds of features can deconstruct and assess PD severity. Finally, by testing a large number of PD samples, it is proved that it is effective and reliable to use the features to assess PD severity.

8. Discussion

In this study, we investigated the process of PD development in simulated GIS under simulated protrusion defect. Moreover, we extracted seven kinds of features that were closely related to PD development. In fact, the characteristics of PD are closely associated with specific insulation defects and environmental factors. Given that the needle-plate models different from the real protrusion defect in GIS and because environmental factors such as trace moisture and temperature are ignored, comprehensive studies on PD development must be conducted under real protrusion defectsand in consideration of environmental factors. Furthermore, we analyzed the microphysical process of PD simply by dividing the charged particles into ions, electrons, and neutral molecules. However, the process of PD involves many complex plasma reactions. To enrich our knowledge of the generation and development of PD, specific physical and chemical reactions in PD must be examined. In addition, certain simulation software can be used to study the PD process under an electric field with alternating current. By extracting the features of different PD stages, we intend to address PD severity in GIS and monitor GIS online. Therefore, the results of this preliminary study can be applied to the assessment of PD severity.

Acknowledgment

The authors acknowledge the fund of The National Basic Research Program of China (973 Program) (2009CB 724506). The National Natural Science Foundation of China (51377181) is also appreciated for supporting this work.

References

[1] M. D. Judd, O. Farish and B. F. Hampton, "The Excitation of UHF Signals by Partial Discharges in GIS," *IEEE Trans. Dielectrics and Electrical Insulation*, vol. 3, no. 2, pp. 213-228, Apr. 1996.

[2] N. van Schaik and T. Czaszejko, "Conditions of Discharge-free Operation of XLPE Insulated Power Cable Systems," *IEEE Trans. Dielectrics and Electrical Insulation*, vol.15, no.4, pp.1120-1130, Aug. 2008.

[3] N. Nagesh and B. I. Gururai, "Evaluation of Digital Filters for Rejecting Discrete Spectral Noise in On-site PD Measurements," *IEEE Trans. Dielectrics and Electrical Insulation*, vol.28, no.1, pp.73-85, Feb. 1993.

[4] Z. R Xu, J. Tang and C. X. Sun, "Application of Complex Wavelet Transform to Suppress White Noise in GIS UHF PD Signals," *IEEE, Trans. Power Delivery*, vol. 22, no. 3, pp. 1498-1504, Jul. 2007.

[5] J. Tang, J. A. Huang, X. X Zhang and C. G. Yao, "Suppression of the Periodic Narrowband Noise with Mixed Frequencies in Partial Discharge On-line Monitoring," *Proceedings of the CSEE*, vol. 30, no. 13, pp. 121-127, May. 2010.

[6] R.V. Maheswari, P. Subburaj, B. Vigneshwaran and M.W. Iruthayarajan, "Partial Discharge Signal Denoising Using Adaptive Translation Invariant Wavelet Transform-online Measurement," *Journal of Electrical Engineering & Technology*, vol. 9, no. 2, pp. 695-706, Mar. 2014.

[7] H. R. Mirzaei, A. Akbari, E. Gockenbach, M. Zanjani, and K. Miralikhani, "A Novel Method for Ultra-high-frequency Partial Discharge Localization in Power Transformers Using the Particle Swarm Optimization Algorithm," *IEEE Electrical Insulation Magazine,* vol. 29, pp. 26-39, Mar.-Apr. 2013.

[8] S. Meijer, E. Gulski and J. J. Smit, "Pattern Analysis of Partial Discharge in SF_6 GIS," *IEEE Trans. Dielectrics and Electrical Insulation*, vol. 5, no. 6, pp. 830-842, Dec. 1998.

[9] H. C. Chen, "Partial Discharge Identification System for High Voltage Power Transformers Using Fractal Feature Based Extension Method," *IET Science, Measurement & Technology*, vol. 7, no. 2, pp. 77-84, Nov. 2013.

[10] W. Y. Chang, "Partial Discharge Pattern Recognition of Cast Resin Current Transformers Using Radial Basis Function Neural Network," *Journal of Electrical Engineering & Technology*, vol. 9, no. 1, pp. 293-300, Jan. 2014.

[11] J. Li, T. Y. Jiang, R. F. Harrison and S. Grzybowski, "Recognition of Ultra High Frequency Partial Discharge Signals Using Multi-scale Features," *IEEE Trans. Dielectrics and Electrical Insulation*, vol. 19, no. 4, pp. 1412-1420, Aug. 2010.

[12] J. Li, R. J. Riao, S. Grzybowski and L. J. Yang, "Oil-paper Aging Evaluation by Fuzzy Clustering and Factor Analysis to Statistical Parameters of Partial Discharges," *IEEE Trans. Dielectrics and Electrical Insulation*, vol. 17, no. 3, pp. 756-763, Jun. 2010.

[13] S. M. Strachan, S. Rudd, , S. D. J. McArthur, M.D. Judd, S. Meijier and E. Gulski, "Knowledge-based Diagnosis of Partial Discharges in Power Transformers," *IEEE Trans. Dielectrics and Electrical Insulation*, vol. 15, no. 1, pp. 259-268, Feb. 2008.

[14] W.G. Chen, C. Wei, Y. Ling and Y.Y. Wang, "Feature Information Extraction of Air-gap Discharge in Oil-paper Insulation and its Process Partition," *Transactions of China Electrotechnical Society*, vol. 26, no. 4, pp. 7-12, Apr. 2011.

[15] W. Z. Chang, C. R. Li, Q. Su and G. Z. Dong, "Study on Development of Partial Discharges at the Defect Caused by a Needle Damage to a Cable Joint," *Proceedings of the CSEE*, vol. 33, no. 7, pp. 192-201, Mar. 2013.

[16] C. X. Wang, Z. G. Tang, W. Z. Chang, S. S. Zheng and C. R. Li, "Experimental Study on Development Characteristics of Point Discharge in GIS," *Power*

System Technology, vol.35, no.11, pp.157-162, Nov. 2011.
[17] B. Qi, C. R Li, B. B. Geng and H. Zhen, "Severity Diagnosis and Assessment of the Partial Discharge Provoked by High-voltage Electrode Defect on GIS Insulator Surface," *IEEE Trans. Power Delivery*, vol. 26, no. 4, pp. 2363-2369, Oct. 2011.
[18] B. Qi , C. R. Li, Z. Hao, B. B. Geng, D. G. Xu, S. Y. Liu and C. Deng, "Surface Discharge Initiated by Immobilized Metal Particles Attach to Gas Insulated Substation Insulators: Process and Feature," *IEEE Trans. Dielectrics and Electrical Insulation*, vol. 183, no. 3, pp. 792-800, Jun. 2011.
[19] X. X. Zhang, J. Tang, W. X. Peng, Y. H. Meng and C. X. Sun, "Study on the Outer UHF Microstrip Patch Antenna for Partial Discharge Detection in GIS," *Chinese Journal of Scientific Instrument*, vol. 27, no. 12, pp. 1595-1599, Dec. 2006.
[20] J. Tang, Q. Zhou and M. Tang, "Study on Mathematical Model for VHF Partial Discharge of Typical Insulated Defects in GIS," *IEEE Trans. Dielectrics and Electrical Insulation*, vol. 14, no. 1, pp. 30-38, Feb. 2007.
[21] X. X. Zhang, J. Z. Tang, J. Tang, Y. Luo and Y. B. Xie, "Relationship Between UHF Signals and Discharge Magnitude from Typical Partial Discharge Defects in GIS," *High Voltage Engineering*, vol. 38, no. 1, pp. 59-65, Jan. 2012.
[22] S. Ohtsuka, T. Teshima, S. Matsumoto and M. Hikita, "Relationship Between PD-induced Electromagnetic Wave Measured with UHF Method and Charge Quantity Obtained by PD Current Waveform in Model GIS," *IEEE Conference on Electrical Insulation and Dielectric Phenomena*, 2006, pp. 615-618.
[23] W. X. Yang and W. T. Peter, "Development of an Advanced Noise Reduction Method for Vibration Analysis Based on Singular Value Decomposition," *NDT & E International*, vol. 36, no. 6, pp. 419-432, Sep. 2003.
[24] H. Wu, "Computer Simulation of Streamer Discharge Process for Gas Insulation in Short Gap," *Master Thesis, North China Electric Power University*, China, Mar. 2012.
[25] R.J. Liao, F. F. Wu, X. H. Liu, F. Yang, L. J. Yang, Z. Zhou, and L. Zhai, "Numerical Simulation of Transient Space Charge Distribution of DC Positive Corona Discharge Under Atmospheric Pressure Air," *Acta Phys. Sin.*, vol. 61, no. 24, 245201, Nov. 2012.
[26] F. F. Wu, R. J. Liao, L. J. Yang and X. H. Liu, Wang Ke, Z. Zhou, "Numerical Simulation of Trichel Pulse Characteristics in Bar-plate DC Negative Corona Discharge," *Acta Phys. Sin.*, vol. 62, no. 11, 115201, Jun. 2013.
[27] C. Cortes, V. Vapnik, "Support-vector Networks," *Machine learning*, vol. 20, no. 3, pp. 273-297, Sep. 1995.

Yu-lin Dong was born in Hengyang City, Hunan Province, China, in 1988. He recieved the Bachelor degree in Huazhong University of Science & Technology, Wuhan, China. He is currently pursuing the Master degree in Chongqing University, Chongqing, China. His reaserch intersts include partial discharge online monitoring and pattern recgnition of GIS.

Ju Tang was born in Pengxi, Sichuan Province, China, in 1960. He received the B.Sc. degree from Xi'an Jiaotong University, Xi'an, China, and the M.sc. and Ph.D degrees from Chongqing University, Chongqing, China. Currently, he is a Professor with The State Key Laboratory of Power Transmission Equipment and System Security and the Chief Scientist presiding over a National Basic Research Program of China (973 Program) (2009CB724506), At present, he is involved in high-voltage equipment online monitoring, fault diagnosis, signal processing, simulation analysis, and pattern recognition. He is a corresponding author in this paper .

Fu-ping Zeng was born in Chongqing, China, in 1984. He received the Bachelor's degree in electrical engineering at Dalian Maritime University, China. He is currently pursuing the Ph.D. degree from the State Key Laboratory of Power Transmission Equipment and System Security and New Technology in Chongqing University, China. He is involved in high-voltage electric equipment insulation online monitoring and fault diagnosis.

Min Liu was born in Huanggang City, Hubei Province, China, in 1979. She received the Bachelor degree and Master degree in Hubei University of Technology in Wuhan city, China, in 2005. after that teaches in transmission line project as a teacher in China Three Gorges University, Yichang city, China, and currently pursuing the doctor degree in Chongqing University, Chongqing, China; her research interests include the online monitoring technology of high voltage equipment.